Optics Letters

Linear mode conversion of terahertz radiation into terahertz surface magnetoplasmons on a rippled surface of magnetized n-InSb

PAWAN KUMAR,[1,*] MANISH KUMAR,[2] AND V. K. TRIPATHI[3]

[1]Department of Physics, Raj Kumar Goel Institute of Technology, Ghaziabad, Uttar Pradesh 201003, India
[2]Department of Electrical Engineering, Indian Institute of Technology, BHU, Varanasi, India
[3]Department of Physics, IIT Delhi, New Delhi 110016, India
*Corresponding author: kumarpawan_30@yahoo.co.in

Received 14 December 2015; revised 18 February 2016; accepted 18 February 2016; posted 22 February 2016 (Doc. ID 255494); published 18 March 2016

A new mechanics of linear mode conversion of terahertz (THz) radiation into THz surface magnetoplasmons on a rippled surface of magnetized n-InSb is proposed. The normally incident THz radiation, polarized in the direction of a ripple wave vector, imparts oscillatory velocity to electrons in the ripple layer. This velocity beats with surface ripple to produce a nonlinear current that resonantly drives the THz surface magnetoplasmons. In the presence of an applied magnetic field, the surface plasmon (SP) mode splits into two modes—an upper mode and a lower mode. The amplitude of the SP for the upper branch mode is higher than that for the lower mode.

OCIS codes: (040.2235) Far infrared or terahertz; (240.6675) Surface photoemission and photoelectron spectroscopy; (240.6680) Surface plasmons; (240.6690) Surface waves; (240.6695) Surface-enhanced Raman scattering.

http://dx.doi.org/10.1364/OL.41.001408

A surface plasmon (SP) is the surface wave propagating at the interface between a conductor and a dielectric or between a conductor and air, with its field amplitude peaking at the interface and falling off exponentially away from it in either medium [1–3]. Due to their highly localized nature at the interface, SPs are extensively used in a number of applications [4–8]. A structured surface significantly slows down the group velocity of SPs and brings the asymptotic SP frequency into the terahertz (THz) frequency range. Such surfaces are called designer plasmonic structures or "spoof" SP structures on metals at THz frequencies [9,10].

The magnetic field is an interesting candidate to control SPs, since it is able to modify the dispersion relation [11–13]. In particular, if the magnetic field is applied parallel to the interface but perpendicular to the SP wave vector, it induces a modification of the SP wave vector while keeping its transverse magnetic (TM) character. Therefore, the magnetic field could be used to control SP propagation, opening the door for novel active plasmonic devices [14–16].

The presence of a static magnetic field may provide additional richness to SPs, turning them into surface magnetoplasmons [17]. Surface magnetoplasmons have been studied in n-InSb, when the magnetic field is parallel to the surface and the direction of propagation is perpendicular to the magnetic field [18]. The coupling of electromagnetic waves with magnetoplasmons has been studied by employing Rayleigh's method [19]. In periodic layers of semiconductors, surface magnetoplasmons have a significant role. The dependence of magnetic force on free electron effective mass is used to characterize the splitting feature of magnetoplasmons with symmetry breaking in the acoustic and optical modes due to the existence of transverse currents induced by the cross polarizations. Spin–orbit interaction enhances the light absorption in plasmonic nanostructures [20]. Subwavelength hole arrays, gratings or nanoslits enhance the extraordinary transmission of THz due to the excitations of SPs, which was studied in terms of various parameters of the subwavelength hole arrays. Enhanced THz transmission was experimentally demonstrated in subwavelength arrays made from both good and poor electrical conductors [5,21–24]. A tunable THz plasmonic subwavelength waveguide based on nonreciprocal surface magnetoplasmons has been proposed by various groups for different structures [25–28].

In this Letter, we propose a new mechanism of linear mode conversion of THz radiation into THz surface magnetoplasmons on a rippled surface of magnetized n-InSb. The magnetic field is perpendicular to the ripple wave vector and the polarization of the incident radiation field. The radiation field imparts oscillatory velocity to electrons in the ripple layer. The surface ripple is equivalent of an electron density ripple. The velocity couples with the density ripple of a suitable wave number to produce a current that resonantly drives the surface magnetoplasmons. The problem is important in the context of THz signal processing, THz sensors and detectors, and active plasmonic devices [14–16] where the appearance of resonance is helpful, and the magnetic field has the ability to tune the surface plasmon resonance (SPR).

Consider a semiconductor–free-space interface $y = 0$ with $y < 0$ being the semiconductor (n-InSb) and $y > 0$ the free space. The semiconductor has static magnetic field $B_s\hat{z}$ (Fig. 1).

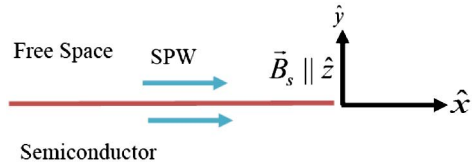

Fig. 1. Schematic of a SP wave propagating along $\hat{x}$ on a semiconductor free space interface, when a static magnetic field exists along $\hat{z}$.

The small free electron effective mass in n-InSb obtains electron plasma frequency, ω_p, in the THz range at lower free electron density and cyclotron resonance at a lower magnetic field. The effective plasma permittivity tensor $\underline{\underline{\varepsilon}}$ of the semiconductor at frequency ω has components

$$\varepsilon_{xx}=\varepsilon_{yy}=(\varepsilon_+ +\varepsilon_-)/2,\quad \varepsilon_{xy}=-\varepsilon_{yx}=(\varepsilon_+ -\varepsilon_-)/2i,$$
$$\varepsilon_{zz}=\varepsilon_L-(\omega_p^2)/(\omega(\omega+i\nu))\quad \varepsilon_+=\varepsilon_L-\omega_p^2/(\omega(\omega-\omega_c+i\nu)),$$
$$\varepsilon_-=\varepsilon_L-\omega_p^2/(\omega(\omega+\omega_c+i\nu)),\quad \varepsilon_{xz}=\varepsilon_{zx}=\varepsilon_{yz}=\varepsilon_{zy}=0,$$

where ε_L is the lattice dielectric constant; $\omega_c=eB_s/mc$ is the electron cyclotron frequency; and $\omega_p=(4\pi n_0 e^2/m)^{1/2}$; e, m, and ν are the charge, effective mass, and collision frequency of electrons, respectively. The interface surface supports SP, which we take to propagate along $\hat{x}$ with t, x dependence of fields as $\exp[-i(\omega t-k_x x)]$. One may write the electric field as

$$\vec{E}=\left(\hat{x}+\frac{ik_x\hat{y}}{\alpha_1}\right)A_0\exp(-\alpha_1 y)\exp[-i(\omega t-k_x x)],\quad \text{for } y>0$$
$$=(\hat{x}+\beta\hat{y})A_0\exp(\alpha_{II}y)\exp[-i(\omega t-k_x x)],\quad \text{for } y<0. \qquad (1)$$

In free space, $k^2=k_x^2-\alpha_I^2=\omega^2/c^2$, hence $\alpha_I^2=k_x^2-\omega^2/c^2$. To obtain E_y we have used $\nabla.\vec{E}=0$. In the magnetized plasma, the extraordinary x-mode dispersion relation is $k^2=k_x^2-\alpha_{II}^2=(\omega^2/c^2)(\varepsilon_{xx}^2+\varepsilon_{xy}^2)/\varepsilon_{xx}$, hence $\alpha_{II}^2=k_x^2-(\omega^2/c^2)(\varepsilon_{xx}^2+\varepsilon_{xy}^2)/\varepsilon_{xx}$. Further, $\nabla\cdot(\underline{\underline{\varepsilon}}\cdot\vec{E})=0$ yields $\beta=-(i\alpha_{II}\varepsilon_{xy}+k_x\varepsilon_{xx})/(\varepsilon_{xy}k_x-i\alpha_{II}\varepsilon_{xx})$. The continuity of the normal component of effective displacement vector $D_{\text{eff}}=(\underline{\underline{\varepsilon}}\bullet\vec{E})_y=(\varepsilon_{XX}E_y-\varepsilon_{xy}E_x)$ across $y=0$ gives the dispersion relation

$$\frac{ik_x}{\alpha_1}=\varepsilon_{xx}\beta-\varepsilon_{xy}=-\frac{k_x\varepsilon_+\varepsilon_-}{k_x\varepsilon_{xy}}-i\alpha_{II}\varepsilon_{xx}. \qquad (2)$$

One may solve Eq. (2) for k_x^2. It gives two roots, corresponding to two surface plasmon eigenmodes:

$$k_x^2=k_{x\pm}^2\equiv\frac{\omega^2}{c^2}\frac{\alpha_2\pm\alpha_3}{\alpha_1}, \qquad (3)$$

where $\alpha_1=\varepsilon_+^2\varepsilon_-^2-2(\varepsilon_{xx}^2-\varepsilon_{xy}^2)+1$, $\alpha_2=\varepsilon_+\varepsilon_-(\varepsilon_+\varepsilon_--\varepsilon_{xx})-\varepsilon_{xx}^2+\varepsilon_{xy}^2+\varepsilon_{xx}$, and $\alpha_3=[\varepsilon_{xy}^2(\varepsilon_{xx}\varepsilon_+\varepsilon_--2\varepsilon_{xx}^2+\varepsilon_{xx})]^{1/2}$.

In the absence of a dc magnetic field, $\vec{B}_s=0$, $\varepsilon_{xy}=0$, $\varepsilon_+=\varepsilon_-=\varepsilon_{xx}$, $\alpha_3=0$, $\alpha_1=(1-\varepsilon_{xx}^2)^2$, and $\alpha_2=\varepsilon_{xx}(1-\varepsilon_{xx})(1-\varepsilon_{xx}^2)$, the two roots coalesce to give the conventional dispersion relation for the SP:

$$k_x^2=\frac{\omega^2}{c^2}\frac{\varepsilon_{xx}}{1+\varepsilon_{xx}}. \qquad (4)$$

The TM field splits the SP into two SP eigenmodes. With the inclusion of collisions, the wave numbers of the upper and lower SP eigenmodes are complex with

$$k_x=k_{xr}+ik_{xi},\qquad k_{xr\pm}=\frac{\omega}{c}\left(\frac{\alpha_{2r}+\alpha_{3r}}{\alpha_{1r}}\right)^{1/2},$$
$$k_{xi\pm}=\frac{\omega^2}{c^2k_{xr\pm}\alpha_{1r}}\left[\alpha_{2i}+\alpha_{3i}-\frac{\alpha_{1i}}{\alpha_{1r}}(\alpha_{2r}+\alpha_{3r})\right].$$

We have carried numerics for the following parameters: $\varepsilon_L=17$, $\nu/\omega_P=10^{-2}$, and $\omega_c/\omega_P=0.05-0.09$. In Fig. 2, we have plotted the normalized real wave numbers of the upper and lower SP eigenmodes $k_{xr\pm}c/\omega_p$ as a function of normalized frequency ω/ω_p. At low frequencies, as one raises the frequency, the wave number increases linearly with nearly identical values for both modes. At higher frequency, the two roots splits, and at large wave numbers the frequency saturates. The saturation frequencies are different for the upper mode (+) and the lower mode (–). In Fig. 3, we have plotted the normalized damping rates $\eta=ck_{xi\pm}c/\omega_p$ as a function of ω/ω_p for $\varepsilon_L=17$, $\nu/\omega_P=10^{-2}$, and $\omega_c/\omega_P=0.06$. The damping rises with frequency. The rise is more rapid for the upper mode (+) as compared to the lower mode (–). As one approaches the saturation frequency, the damping becomes severe.

Now we allow a surface ripple on the semiconductor (Fig. 4), $qh\geq 1$, where q is the ripple wave vector and h is the amplitude of the ripple. The presence of the surface ripple provides unmatched momentum. As one moves along $\hat{x}$ in the ripple region $y=h\cos qx$, the electron density shows a periodic variation with x; hence, we model the surface ripple as a density ripple with density [29]

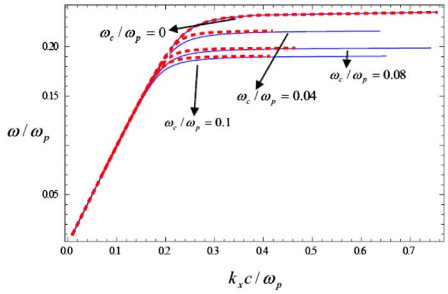

Fig. 2. Dispersion relation of n-InSb for a SP in the collisionless regime for (upper mode (+), red) and (lower mode (–), blue) modes for parameters $\epsilon_L=17$, $\nu/\omega_P=10^{-2}$, and $\omega_c/\omega_P=0.05-0.09$.

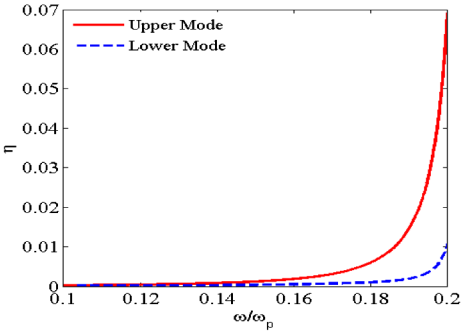

Fig. 3. Normalized damping rates $\eta=ck_{xi\pm}c/\omega_p$ as a function of ω/ω_p for $\epsilon_L=17$, $\nu/\omega_P=10^{-2}$, and $\omega_c/\omega_P=0.06$.

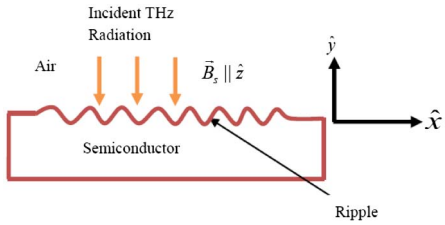

Fig. 4. THz radiation is normally incident on the rippled surface.

$$n_0 = \frac{n_0^0}{2} + n_q, \qquad n_q = \frac{n_0^0}{2}\cos qx. \tag{5}$$

A THz electromagnetic wave, with electric field

$$\vec{E}_0 = \hat{x}A_0 e^{-i\left(\omega t + \frac{\omega}{c}\hat{y}\right)}, \tag{6}$$

is normally incident on it. The transmitted field, on ignoring the effect of the ripple, can be written as

$$\vec{E}_T = (\hat{x} + \beta_1\hat{y})TA_0 e^{-i\omega t}e^{\alpha y}, \tag{7}$$

where $\alpha = (\omega/c)((-\varepsilon_+\varepsilon_-)/\varepsilon_{xx})^{1/2}$ and $\beta_1 = \varepsilon_{xy}/\varepsilon_{xx}$, in compliance with Maxwell's equation $\nabla\cdot(\underline{\underline{\varepsilon}}\cdot\vec{E}) = 0$. The magnetic field of the transmitted wave using $\vec{B} = (c/i\omega)\nabla\times\vec{E}$, can be written as

$$\vec{B}_T = -\hat{z}TA_0\frac{c\alpha}{i\omega}e^{-i\omega t}e^{\alpha y}. \tag{8}$$

Using the continuity of E_x and B_z at $y = 0$, one obtains the amplitude transmission coefficient $T = 2/(1 + i\alpha c/\omega)$. The transmitted field imparts oscillatory velocity to electrons. Solving the equation of motion, $m(\partial\vec{v}/\partial t) = -e\vec{E}_T - (e/c)\vec{v}\times\vec{B}_s - m\vec{v}\nu$, one obtains

$$\vec{v} = \frac{e}{m((\omega + i\nu)^2 - \omega_c^2)}(-i(\omega + i\nu)\vec{E}_T - \omega_c\vec{E}_T\times\hat{z}). \tag{9}$$

In the ripple region $(-h < y < h)$, $\vec{v}$ couples with the density ripple n_q to produce the nonlinear current density at $(\omega, q\hat{x})$

$$\vec{J}^{\mathrm{NL}} = -\frac{en_q\vec{v}}{2} = -\frac{e^2n_0^0}{4m((\omega + i\nu)^2 - \omega_c^2)} \times(-i(\omega + i\nu)\vec{E}_T - \omega_c\vec{E}_T\times\hat{z})e^{iqx}. \tag{10}$$

In the ripple region, $e^{\alpha y} \approx 1$. The current density resonantly excites a SP of frequency ω, when q equals the SP wave vector given by Eq. (4), $q = k_{xr+}$ or $q = k_{xr-}$, where $k_{xr\pm}$ are the real parts of $k_{x\pm}$. Let us consider the excitation of the upper mode (+). The wave equation governing the SP, on using Maxwell's equations $\nabla\times\vec{E} = (i\omega/c)H$ and $\nabla\times\vec{H} = -(i\omega/c)\underline{\underline{\varepsilon}}\cdot\vec{E} + (4\pi/c)\vec{J}^{\mathrm{NL}}$, can be written as

$$\nabla^2\vec{E} - \nabla(\nabla\cdot\vec{E}) + \frac{\omega^2}{c^2}\underline{\underline{\varepsilon}}\cdot\vec{E} = -\frac{4\pi i\omega}{c^2}\vec{J}^{\mathrm{NL}}. \tag{11}$$

From the y component of Eq. (11) we get

$$E_y = \frac{\left(\frac{\omega^2}{c^2}\varepsilon_{xy} + iq\frac{\partial}{\partial y}\right)}{\left(\frac{\omega^2}{c^2}\varepsilon_{xx} - q^2\right)}E_x. \tag{12}$$

For the x component, Eq. (11) gives

$$\frac{\partial^2E_x}{\partial y^2} - k_y^2E_x = -\frac{4\pi i}{\omega\varepsilon_{xx}}\left(\frac{\omega^2}{c^2}\varepsilon_{xx} - q^2\right)J_x^{\mathrm{NL}}, \tag{13}$$

where $k_y^2 = q^2 - (\omega^2/c^2)(\varepsilon_{xx}^2 + \varepsilon_{xy}^2)/\varepsilon_{xx}$ for $y < 0$ and $k_y^2 = q^2 - \omega^2/c^2$ for $y > 0$. When the current source is neglected, one obtains

$$\frac{\partial^2E_x}{\partial y^2} - k_y^2E_x = 0. \tag{14}$$

The solution for Eq. (14) is given as

$$\vec{E} = A\vec{\psi}(y)e^{-i(\omega t - qx)}, \tag{15}$$

where

$$\vec{\psi}(y) = \left(\hat{x} + i\frac{q}{\alpha_I}\hat{y}\right)e^{-\alpha_I y} \quad \text{for } y > 0,$$
$$= (\hat{x} + \beta\hat{y})e^{\alpha_{\mathrm{II}}y} \quad \text{for } y < 0.$$

When the current source is retained, we assume that the mode structure of the surface wave is not modified, and write

$$\vec{E} = A(x)\vec{\psi}(y)e^{-i(\omega t - qx)}. \tag{16}$$

Using Eqs. (13) and (16) and letting $q- > q - i\partial/\partial x$, one obtains

$$2iq\vec{\psi}(y)\frac{\partial A(x)}{\partial x} - 2ik_{xr+}k_{xi+}A(x)\vec{\psi}(y) = -\frac{4\pi i}{\omega\varepsilon_{xx}}\left(\frac{\omega^2}{c^2}\varepsilon_{xx} - q^2\right)\vec{J}^{\mathrm{NL}}. \tag{17}$$

where k_{xi+} is the imaginary part of k_{x+}. Multiplying Eq. (17) by $\psi^*(y)dy$ and integrating from $-\infty$ to $+\infty$, one obtains

$$\frac{\partial A}{\partial x} + k_{xi+}A = -\frac{2\pi}{q\omega\varepsilon_{xx}}\left(\frac{\omega^2}{c^2}\varepsilon_{xx} - q^2\right) \times\frac{\int_{-\infty}^{\infty}\vec{\psi}^*(y)\cdot\vec{J}^{\mathrm{NL}}\mathrm{d}y}{\int_{-\infty}^{\infty}\vec{\psi}(y)\cdot\vec{\psi}^*(y)\mathrm{d}y}e^{i(\omega t - qx)}. \tag{18}$$

If one ignores the absorption of the SP, Eq. (18) integrates, over the length of illumination d, to give

$$\frac{A}{A_0} = \frac{1}{4}\left(\frac{\omega_p^2}{(\omega + i\nu)^2 - \omega_c^2}\right)\left(\frac{\frac{\omega^2}{c^2}\varepsilon_{xx} - q^2}{q\omega\varepsilon_{xx}}\right) \times\left(i(\omega + i\nu)\left(2 + \frac{i\beta_1 q}{\alpha_I} + \beta\beta_1\right) + \omega_c\left(2\beta_1 - \beta - \frac{iq}{\alpha_I}\right)\right)\left(\frac{1}{\frac{1+(q/\alpha_I)^2}{\alpha_I} + \frac{1+\beta^2}{\alpha_{\mathrm{II}}}}\right)dhT. \tag{19}$$

When $d > 1/k_{xi+}$, where k_{xi+} is the imaginary part of k_{x+}, Eq. (19) still holds with d replaced by $1/k_{xi+}$. In Fig. 5, we have plotted normalized THz amplitude versus normalized frequency for the upper and lower modes of a SP for the parameters $\varepsilon_L = 17$, $\nu/\omega_p = 0.014$, $d\omega_p/c = 5$, $\omega/\omega_p = 0.05$–0.25, and $\omega_c/\omega_p = 0.08, 0.04, 0.1$. This shows that the amplitude of the SP for the upper mode is higher than that for the lower mode, because the upper mode has a lower wave number than the lower mode, and the amplitude is inversely proportional to the wave number. In Fig. 6, we have plotted normalized THz amplitude versus the normalized electron cyclotron frequency for the upper and the lower modes of SPs for the parameters $d\omega_p/c = 5$, $\varepsilon_L = 17$, and $\omega_c/\omega_p = 0$ – 0.1. As seen from the figures, as one increases the magnetic field,

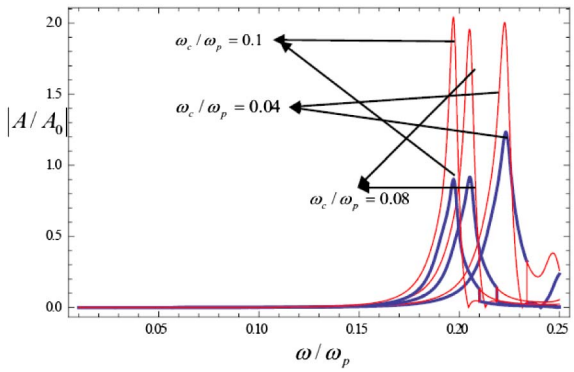

Fig. 5. Normalized amplitude of THz SP wave versus normalized electron cyclotron frequency for the upper (red) and lower (blue) modes for the parameters $\epsilon_L = 17$, $\nu/\omega_p = 0.014$, $d\omega_p/c = 5$, and $\omega/\omega_p = 0.05 - 0.25$.

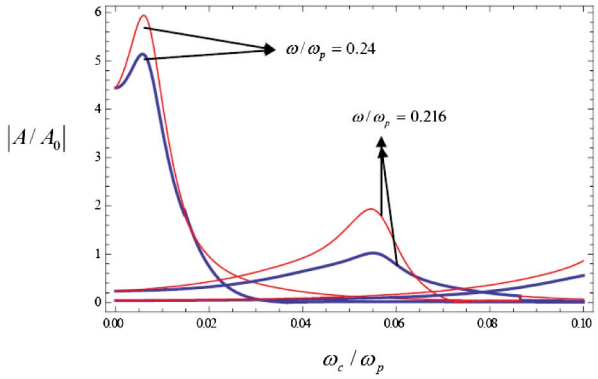

Fig. 6. Plot of normalized THz amplitude versus normalized SP wave frequency for the upper mode (red) and lower mode (blue) for the parameters $\epsilon_L = 17$, $\nu/\omega_p = 0.014$, $d\omega_p/c = 5$, and $\omega_c/\omega_p = 0 - 0.1$.

the cut-off frequency of the SP decreases, and, at a specified magnetic field, the SP at the corresponding cut-off frequency is generated.

The TM field splits the SP into two modes. The cut-off frequencies for both SP modes decrease with increasing magnetic field. At a given free electron density (say, $n_0 \approx 2.4 \times 10^{18}$ cm^{-3}), and a specific magnetic field and ripple wave number, the SP amplitude has a sharp maximum at a given frequency for which the phase matching condition is satisfied. As one increases the magnetic field, this optimum frequency decreases for the cases of both the upper and lower modes.

In conclusion, the amplitude of a SP for the upper mode is higher than that for the lower mode. This is because the upper mode has a lower wave number than the lower mode, and the amplitude is inversely proportional to the wave number. The inverse dependence of the THz amplitude on wave number arises due to the $\partial^2 E/\partial z^2$ term in the wave equation, which is replaced by $(-k_z^2 A + 2ik_z \partial A/\partial z) \exp[-i(\omega t - k_z z)]$; $k_z = q$. The $k_z^2 A$ term cancels with the other terms, hence, $\partial A/\partial z$ goes as $1/k_z$, leading to $A \sim 1/k_z$. Physically, this means that rapid phase variations in z reduce the spatial growth of the wave amplitude. For a given q, the frequency of the laser that would resonantly mode convert to a SP varies with ω_c. Thus, by varying ω_c, one can mode convert the THz of different ω. The electron density in InSb is $n_0 \approx 2.4 \times 10^{18}$ cm^{-3}, so the highest possible frequency of a SP at a semiconductor–vacuum interface is around 6 THz. Mid-IR SPs would not exist in this proposed device. The case of a n-InSb surface with an array of holes should be similar to the surface ripple, as the holes bring a sudden discontinuity in electron density. The wave number of the ripple, for a given electron density, is the same as that of the SP given in Eq. (4).

REFERENCES

1. R. H. Ritchie, Phys. Rev. **106**, 874 (1957).
2. H. Raether, *Surface Plasmons on Smooth and Rough Surfaces and on Gratings*, Springer Tracts in Modern Physics (Springer, 1988).
3. L. Barnes, A. Dereux, and T. W. Ebbesen, Nature **424**, 824 (2003).
4. J. Homola, S. S. Yee, and G. Gauglitz, Sens. Actuators B **54**, 3 (1999).
5. T. W. Ebbesen, H. J. Lezec, H. F. Ghaemi, T. Thio, and P. A. Wolff, Nature **391**, 667 (1998).
6. S. M. Nie and S. R. Emery, Science **275**, 1102 (1997).
7. S. A. Maier, S. R. Andrews, L. Martın-Moreno, and F. J. Garcıa-Vidal, Phys. Rev. Lett. **97**, 176805 (2006).
8. P. Kumar, V. K. Tripathi, and C. S. Liu, J. Appl. Phys. **104**, 033306 (2008).
9. J. B. Pendry, L. Martin-Moreno, and F. J. Garcia-Vidal, Science **305**, 847 (2004).
10. C. R. Williams, S. R. Andrews, S. A. Maier, A. I. Fernández-Domínguez, L. Martín-Moreno, and F. J. García-Vidal, Nat. Photonics **2**, 175 (2008).
11. C. Clavero, K. Yang, J. R. Skuza, and R. A. Lukaszew, Opt. Lett. **35**, 1557 (2010).
12. S. Fan, Nat. Photonics **4**, 76 (2010).
13. S. Cinà, D. M. Whittaker, D. D. Arnone, T. Burke, H. P. Hughes, M. Leadbeater, M. Pepper, and D. A. Ritchie, Phys. Rev. Lett. **83**, 4425 (1999).
14. K. F. MacDonald, Z. L. Sámson, M. I. Stockman, and N. I. Zheludev, Nat. Photonics **3**, 55 (2008).
15. V. V. Temnov, G. Armelles, U. Woggon, D. Guzatov, A. Cebollada, A. Garcia-Martin, J.-M. Garcia-Martin, T. Thomay, A. Leitenstorfer, and R. Bratschitsch, Nat. Photonics **4**, 107 (2010).
16. V. Kuzmiak, S. Eyderman, and M. Vanwolleghem, Phys. Rev. B **86**, 045403 (2012).
17. M. S. Kushwaha, Surf. Sci. Rep. **41**, 1 (2001).
18. J. J. Brion, R. F. Wallis, A. Hartstein, and E. Burstein, Phys. Rev. Lett. **28**, 1455 (1972).
19. N. E. Glass, Phys. Rev. B **41**, 7615 (1990).
20. J. Soni, S. Ghosh, S. Mansha, A. Kumar, S. Dutta Gupta, A. Banerjee, and N. Ghosh, Opt. Lett. **38**, 1748 (2013).
21. W.-C. Tan, T. W. Preist, and R. J. Sambles, Phys. Rev. B **62**, 11134 (2000).
22. D. Qu and D. Grischkowsky, Phys. Rev. Lett. **93**, 196804 (2004).
23. A. K. Azad and W. Zhang, Opt. Lett. **30**, 2945 (2005).
24. M. A. Seo, H. R. Park, S. M. Koo, D. J. Park, J. H. Kang, O. K. Suwal, S. S. Choi, P. C. M. Planken, G. S. Park, N. K. Park, Q. H. Park, and D. S. Kim, Nat. Photonics **3**, 152 (2009).
25. B. Hu, Q. J. Wang, and Y. Zhang, Opt. Lett. **37**, 1895 (2012).
26. F. Fan, S. Chen, X.-H. Wang, and S. J. Chang, Opt. Express **21**, 8614 (2013).
27. F. Fan, S. Chen, W. Lin, Y.-P. Miao, S. J. Chang, B. Liu, X.-H. Wang, and L. Lin, Appl. Phys. Lett. **103**, 161115 (2013).
28. S. Chen, F. Fan, X. H. Wang, P. Wu, H. Zhang, and S. J. Chang, Opt. Express **23**, 1015 (2015).
29. C. S. Liu and V. K. Tripathi, IEEE Trans. Plasma Sci. **28**, 353 (2000).